Steel and Composite Structures, *Vol. 35, No. 4 (2020) 555-566*
DOI: https://doi.org/10.12989/scs.2020.35.4.555

Stability of perforated nanobeams incorporating surface energy effects

Khalid H. Almitani [1a], Alaa A. Abdelrahman[2b] and Mohamed A. Eltaher[*1,2]

[1]Department of Mechanical Engineering, Faculty of Engineering, King Abdulaziz University, P.O. Box 80204, Jeddah, Saudi Arabia
[2]Department of Mechanical Design & Production, Faculty of Engineering, Zagazig University, P.O. Box 44519, Zagazig, Egypt

(*Received February 5, 2020, Revised April 4, 2020, Accepted April 14, 2020*)

Abstract. This paper aims to present an analytical methodology to investigate influences of nanoscale and surface energy on buckling stability behavior of perforated nanobeam structural element, for the first time. The surface energy effect is exploited to consider the free energy on the surface of nanobeam by using Gurtin-Murdoch surface elasticity theory. Thin and thick beams are considered by using both classical beam of Euler and first order shear deformation of Timoshenko theories, respectively. Equivalent geometrical constant of regularly squared perforated beam are presented in simplified form. Problem formulation of nanostructure beam including surface energies is derived in detail. Explicit analytical solution for nanoscale beams are developed for both beam theories to evaluate the surface stress effects and size-dependent nanoscale on the critical buckling loads. The closed form solution is confirmed and proven by comparing the obtained results with previous works. Parametric studies are achieved to demonstrate impacts of beam filling ratio, the number of hole rows, surface material characteristics, beam slenderness ratio, boundary conditions as well as loading conditions on the non-classical buckling of perforated nanobeams in incidence of surface effects. It is found that, the surface residual stress has more significant effect on the critical buckling loads with the corresponding effect of the surface elasticity. The proposed model can be used as benchmarks in designing, analysis and manufacturing of perforated nanobeams.

Keywords: surface energy effects; perforated nanobeams; thin and thick beams; non-classical; buckling; analytical solution

1. Introduction

Nanotechnology is primarily concerned with fabrication of nanostructure elements (i.e., nanobars, nanobeams, nanoplates, and nanoshells), which enables a new generation of devices and systems with revolutionary properties and enhanced functionality. The understanding of mechanical behavior of nanostructures is essential in the development of such structures for engineering applications. Among these nanostructures are nanobeams that attract more and more attention due to their great potential engineering applications, such as nanowires, nano-probes, micro/nano-electromechanical systems (MEMS and NEMS), atomic force microscope (AFM), nanoactuators and nanosensors, Eltaher *et al.* (2013). Nanobeams are prone to buckling when they are subjected to inplane compressive forces. References dealing with buckling can be classified into two categories: the first is concerned with the linear buckling problem and the second is concerned with the nonlinear buckling problem. Within the linear buckling analysis, the main outcome is to find the critical buckling loads and the associated mode shapes, Eltaher *et al.* (2016a).

Fu *et al.* (2010) illustrated influences of the surface energies on the static buckling and dynamic behaviors of geometry nonlinear nanobeams by using Galerkin method. Ansari and Sahmani (2011) developed a non-classical solution to analyze bending and buckling responses of nanobeams including surface stress effects. Wang (2012) studied post-buckling behavior of supported nanobeams containing internal flowing fluid with two surface layers based on a nonlinear theoretical model. Eltaher *et al.* (2013a, 2014a) analyzed static and buckling behaviors of functionally graded Euler and Timoshenko nonlocal nanobeams by using finite element method. Eltaher (2014b) figured out effective of higher order strain gradient nanobeam model in analysis of static buckling stability of nanobeams. Sedighi and Daneshmand (2014) studied nonlinear transversely vibrating beams by the homotopy perturbation method with an auxiliary term. Khater *et al.* (2014) presented the impact of surface energy and thermal loading on the static stability of nanowires modeled as curved fixed–fixed Euler-Bernoulli beam. Oveissi *et al.* (2015) investigated axial wave propagation of CNTs conveying fluid. Chaht *et al.* (2015) addressed theoretically the bending and buckling behaviors of size-dependent nanobeams made of functionally graded materials (FGMs) including the thickness stretching effect based on the nonlocal continuum model. Sedighi and Bozorgmehri (2016) studied dynamic instability analysis of doubly clamped cylindrical nanowires in the presence of Casimir attraction and surface effects using modified couple stress

*Corresponding author, Professor
E-mail: meltaher@kau.edu.sa
[a]Ph.D.
E-mail: kalmettani@kau.edu.sa
[b]Ph.D.
E-mail: alaa.ahmed@zu.edu.eg;

ISSN: 1229-9367 (Print), 1598-6233 (Online)

theory. Eltaher *et al.* (2016b) illustrated effects of thermal load and shear force on the buckling of nonlocal nanobeams by using higher-order beam theories. Ahouel *et al.* (2016) developed a nonlocal trigonometric shear deformation beam theory based on neutral surface position for bending, buckling, and vibration of FG nanobeams using the nonlocal differential constitutive relations of Eringen.

Oveissi *et al*. (2016a, b, 2017) studied longitudinal and transverse vibrations and instabilities of CNTs conveying fluid considering size effects of nanoflow and nanostructure. Ouakad *et al*. (2017) investigated nonlinear internal resonances of MEMS arch excited by static (DC) and dynamic (AC) electric forces. Shen *et al*. (2017) developed a microstructure-dependent dynamic model for silicon nanobeams with axial motion by considering the effects of nonlocal elasticity and surface energy. Ebrahimi *et al*. (2017) developed modified continuum model by using Gurtin-Murdach surface energy theory to investigate free vibration and buckling behaviors of nanobeams. Saffari *et al.* (2017) studied dynamic stability of functionally graded nanobeam based on nonlocal Timoshenko theory considering surface effects. Bellifa *et al*. (2017) developed nonlocal zeroth-order shear deformation theory in analysis of nonlinear postbuckling behavior of nanoscale beams. Mercan and Civalek (2017) investigated stability of the Silicon carbide nanotube in the static buckling case with surface effect and nonlocal continuum theory. Mirkalantari *et al.* (2017) developed a modified continuum model based on strain gradient and surface stress effect to study pull-in instability analysis of rectangular nanoplate. Based on the nonlocal elasticity differential model of Eringen and nonlinear Bernoulli-Euler beam theory, Emam *et al*. (2018) studied the postbuckling and free vibration response of geometrically imperfect multilayer nanobeams subjected to a pre-stress compressive load. Foroutan *et al*. (2018) analyzed buckling of current-carrying nanowires in the presence of a longitudinal magnetic field accounting for both surface and nonlocal effects. Mohammadimehr *et al.* (2018) explored static, buckling and free vibration behaviors of a micro compositebeam reinforced by single-walled carbon nanotubes (SWCNTs) with considering temperature-dependent material properties and surface effect properties. Oveissi *et al.* (2018) investigated effects of axially moving carbon nanotube, nanoflow, and Knudsen number on the vibrational behavior of the system by using nonlocal elasticity. Almitani (2018) studied buckling characteristics of both nonlinear symmetric power and sigmoid FG beams.

Mohamed *et al.* (2019) and Eltaher *et al.* (2019) investigated buckling and post-buckling behaviors of imperfect single walled carbon nanotube (SWCNT) modeled as a beam structure by using energy-equivalent model to include the size scale effect. Barati and Zenkour (2019) studied thermal post-buckling of a geometrically imperfect nanoscale piezoelectric beam under closed circuit condition accounting for the flexoelectricity and surface effects. Hashemian *et al*. (2019a) presented comprehensive beam models for buckling and bending behavior of simple nanobeam based on nonlocal strain gradient theory and surface effects. Hashemian *et al*. (2019b) investigated viscous fluid flow and dynamic stability of CNTs subjected to axial harmonic load coupled using Bolotin's method. Benahmed *et al.* (2019) derived analytically critical buckling loads of FG nanoscale beam with porosities using nonlocal higher-order shear deformation. Esmaeili and Beni (2019) examined buckling and vibration behaviors of FG flexoelectric nanobeam. Jena *et al*. (2019) presented effects of surface energy and surface residual stresses on the stability of different types of SWCNTs rested in Winkler elastic foundations and exposed to the low and high temperature environments. Yousefzadeh *et al.* (2019) analyzed buckling of a multi-layered nanocomposite rectangular plate reinforced by SWCNTs rested on elastic medium considering nonlocal theory of Eringen.

Mohamed *et al*. (2020) studied buckling and post-buckling of SWCNT by using energy-equivalent model and higher order shear deformation of beam. Hamidi *et al.* (2020) presented theoretical analysis of thermoelastic damping of silver nanobeam resonators based on Green–Naghdi via nonlocal elasticity with surface energy effects. Khabaz *et al.* (2020) presented optimal vibration control of multi-layer micro-beams actuated by piezoelectric layer based on modified couple stress and surface stress elasticity theories. Eltaher *et al.* (2020a) and Hamed *et al.* (2020) studied the buckling of composite beam structure with and without elastic foundation under varying axial load. Hadipeykani *et al.* (2020) predicted the glass transition temperature and volumetric thermal expansion coefficient of thermoset polymer-based epoxy nanocomposite reinforced by CNT by using molecular dynamics simulation. Malikan and Eremeyev (2020) predicted theoretically post-critical axial buckling behavior of conical carbon nanotubes based on the Euler-Bernoulli beam model, Lagrangian strains, and nonlocal strain gradient theory, and surface effect. Pirmoradian *et al.* (2020a) investigated thermo-mechanical stability of single-layered graphene sheets embedded in an elastic medium under action of a moving nanoparticle. Pirmoradian *et al.* (2020b) studied the effect of size-dependent on vibration and stability of DWCNTs subjected to moving nanoparticles and embedded on two-parameter foundations.

Etching holes, perforation and cutouts of structures are compulsory in some modern applications such as in heat exchangers, nuclear power plants, filtration and microeletromicanical system (MEMS), Almitani *et al.* (2019). In micro and nanostructures, perforation is often necessary for sacrificial-layer removal, representing a technological constraint for the designer, De Pasquale et al. (2010). The perforated beam and plates of MEMS are used to reduce the gas forces of oscillating structures, the squeeze film damping, and increase the switching speed, Rebeiz (2003). Further analysis reveals that perforated structure improves the switching time of the switch and also affects the capacitance of the switch, Bendali *et al*. (2006). Luschi and Pieri (2014, 2016) developed closed expressions for the equivalent bending and shear stiffness of clamped–clamped beams with regular square perforations and determined their resonance frequencies. Guha *et al.* (2015) developed a modified capacitance model of RF MEMS shunt switch incorporating fringing field effects of perforated beam. Bourouina *et al*. (2016) investigation of thermal loads and small-scale effects on free dynamics vibration of slender simply supported nonlocal perforated nanobeams with periodic square holes network. Guha *et al.* (2017) presented novel analytical model for optimizing the pull-in voltage in a flexure MEMS switch incorporating beam perforation effect. Eltaher *et al*. (2018a, b) developed an analytical model capable of predicting bending response, critical buckling loads and natural frequencies of perforated thin and thick nanobeams by using nonlocal differential form of Eringen model. Abdelrahman *et al*. (2019) and Almitani *et al.* (2019) studied the free and forced vibration of perforated beam with regular array of squares by using analytical method and derived closed forms for resonant frequencies, corresponding Eigen-mode functions. Rao *et al.* (2019) presented new analytical capacitance modeling of the perforated switch considering the fringing effect. Kerid *et al*. (2019) explored the magnetic field, thermal loads and small-scale effects on the dynamic vibration of Euler–Bernoulli nanobeam structure composed of a rectangular configuration perforated with periodic square holes network and subjected to axial magnetic field. Bourouina *et al*. (2020) illustrated the influence of hole networks on the adsorption-induced frequency shift of a nonlocal perforated nanobeam. Eltaher and Mohamed (2020) derived closed form solution to evaluate the natural frequencies and mode shapes of nonlocal perforated nanobeams under general boundary conditions. Eltaher *et al*. (2020b) studied bending and vibration of piezoelectric nonlocal Euler-Bernoulli nanobeam with cutouts by using finite element method.

Corresponding to author's information, the analysis of static stability of perforated nanobeam with nanoscale and surface energy has not be considered elsewhere. So, this manuscript tends to fill this gap and present a unified comprehensive model including surface energy effects to study a buckling of perforated nanostructure. The manuscript is ordered as follows: equivalent geometrical and material properties of beams perforated are described in section 2. Kinematic relations, surface elasticity, nonlocal constitutive equations, and equilibrium equations of thin and thick perforated nanobeam are presented in section 3. Analytical solutions for critical buckling load of perforated nanobeam including surface effects are presented in section 4. Model validation and parametric studies to present influences of filling ratio, the number of hole rows, surface material characteristics, beam slenderness ratio as well as the boundary conditions on the critical buckling loads are presented in section 5. Discussion and main points are summarized in Section 6.

2. Geometrical modification

Consider a regularly squared perforated nanobeam has the following geometrical characteristics: length L, thickness h, and width w. The regular squared pattern of perforation has the following characteristics: the spatial perforation period l_s, hole side $l_s - t_s$, and the number of holes throughout the cross section is N, as shown in Fig. 1.

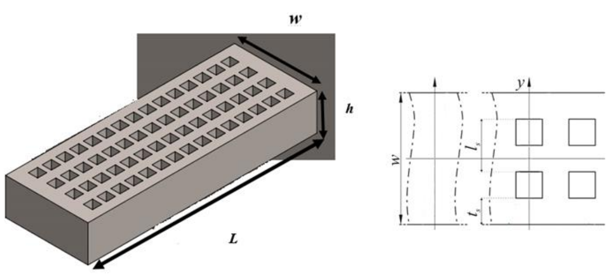

Fig. 1 A perforated beam with the geometrical parameters Eltaher and Mohamed (2020)

The perforated beam filling ratio (α) can be expressed as

$$\alpha = \frac{t_s}{l_s}, \qquad 0 < \alpha \le 1 \tag{1}$$

where t_s is spatial period, and l_s spatial perforation period. Assume that the total induced stress throughout the cross section is the same for both fully filled solid nanobeam and the corresponding perforated one. Also, the stress distribution throughout the filled segment in the perforated nanobeam is assumed to be linear and continuous.

So, the equivalent bending stiffness and shear stiffness can be represented by Abdelrahman *et al.* (2019)

$$\begin{aligned}(EI)_{Perf} = (EI)_{Solid}[\alpha(N+1)(N^2+2N+\alpha^2) \\ /((1-\alpha^2+\alpha^3)N^3+3\alpha N^2+ \\ (3+2\alpha-3\alpha^2+\alpha^3)\alpha^2 N+\alpha^3)]\end{aligned} \tag{2a}$$

$$(GA)_{perf} = (GA)_{solid}[(\alpha^3(N+1))/2N] \tag{2b}$$

in which E and G are the elasticity modulus and shear modulus of the fully filled beam material, A and I are the area and the second moment of area of the fully filled beam. The equivalent mass $[(\rho A)_{Perf}]$ and moment of inertia $[(\rho I)_{perf}]$ per unit length of the perforated nanobeam can be also expressed by Eltaher *et al*. (2018a,b)

$$(\rho A)_{Perf} = (\rho A)_{solid}\left\{\frac{[1-N(\alpha-2)]\alpha}{N+\alpha}\right\} \tag{3a}$$

$$(\rho I)_{perf} = (\rho I)_{solid}\left\{\begin{aligned}\frac{\alpha(2-\alpha)N^3+3N^2}{(N+\alpha)^3}- \\ \frac{2\alpha(\alpha-3)(\alpha^2-\alpha+1)N+\alpha^2+1}{(N+\alpha)^3}\end{aligned}\right\} \tag{3b}$$

Assuming small unit cells and N>>1, the equivalent mass density is obtained by averaging the unit cell mass over its volume, thus giving, Luschi and Pieri (2016)

$$(\rho)_{Perf} = (\rho)_{solid}\{[(2-\alpha)]\alpha\} \tag{4}$$

From Eqs. (3) and (4) the equivalent cross-sectional area and 2nd moment of area of perforated nanobeam are

$$(A)_{Perf} = \frac{(\rho A)_{solid}}{(\rho)_{Perf}} \left\{ \frac{[1-N(\alpha-2)]\alpha}{N+\alpha} \right\} = (A)_{solid} \left\{ \frac{[1-N(\alpha-2)]}{(N+\alpha)(2-\alpha)} \right\} \quad (5a)$$

$$(I)_{perf} = (I)_{solid} \left\{ \frac{(2-\alpha)N^3 + 3N^2}{(2-\alpha)(N+\alpha)^3} - \frac{2(\alpha-3)(\alpha^2-\alpha+1)N + \alpha^2 + 1}{(2-\alpha)(N+\alpha)^3} \right\} \quad (5b)$$

Consequently, the equivalent geometrical characteristics of the surface layer can be expressed as

$$(A\tau_s)_{perf} = (A\tau_s)_{solid} \left\{ \frac{[1-N(\alpha-2)]}{(N+\alpha)(2-\alpha)} \right\} \quad (6)$$

in which τ_s is the surface residual stress.

3. Mathematical formulation

In this section, the mathematical formulation of perforated nanobeams considering surface energy effects is presented through this section. Both Euler Bernoulli beam theory (EBBT) and Timoshenko beam theory, (TBT) are considered throughout this study.

3.1 Strain-Displacement relation

The displacement field of beam generalized beam theory can be depicted in a general form as

$$u_x(x,z,t) = u_o(x,t) - z\frac{\partial w(x,t)}{\partial x} + \gamma(z)\left(\frac{\partial w(x,t)}{\partial x} + \Phi(x,t)\right) \quad (7a)$$

$$u_z(x,z,t) = w(x,t) \quad (7b)$$

where u_x, and u_z are the total displacements along the coordinate directions (x, z), and u_o, w, and Φ denote the axial, transverse and angular displacements of a point on the neutral axis. While $\gamma(z)$ is the beam shape function which can be written as, Ansari and Sahmani (2011)

$$\gamma(z) = 0 \quad (EBBT) \quad \& \quad \gamma(z) = z \quad (TBT) \quad (8)$$

Using the linear strain-displacement relations, the components of normal strain ε_{xx}, shear strain, ε_{xz} are, Yang *et al.* (2002), Ansari and Sahmani (2011)

$$\varepsilon_{xx}(x,t) = \begin{cases} \dfrac{\partial u_o(x,t)}{\partial x} - z\dfrac{\partial^2 w(x,t)}{\partial^2 x} & (EBBT) \\ \dfrac{\partial u_o(x,t)}{\partial x} + z\dfrac{\partial \Phi(x,t)}{\partial x} & (TBT) \end{cases} \quad (9a)$$

$$\varepsilon_{xz}(x,t) = \begin{cases} 0 & (EBBT) \\ \dfrac{1}{2}\left(\dfrac{\partial \mathrm{w}(x,t)}{\partial x} + \Phi(x,t)\right) & (TBT) \end{cases} \quad (9b)$$

3.2 Constitutive equations

Considering the Poisson's effect, the constitutive equations are given by, Yang *et al.* (2002)

$$\sigma_{xx} = \begin{cases} \dfrac{(1-\nu)E}{(1+\nu)(1-2\nu)}\left(\dfrac{\partial u_o(x,t)}{\partial x} - z\dfrac{\partial^2 \mathrm{w}(x,t)}{\partial x^2}\right) & (EBBT) \\ \dfrac{(1-\nu)E}{(1+\nu)(1-2\nu)}\left(\dfrac{\partial u_o(x,t)}{\partial x} + z\dfrac{\partial \Phi(x,t)}{\partial x}\right) & (TBT) \end{cases} \quad (10a)$$

$$\sigma_{yy} = \sigma_{zz} = \begin{cases} \lambda\left(\dfrac{\partial u_o(x,t)}{\partial x} - z\dfrac{\partial^2 \mathrm{w}(x,t)}{\partial x^2}\right) = \left(\dfrac{\nu}{1-\nu}\right)\sigma_{xx} & (EBBT) \\ \lambda\left(\dfrac{\partial u_o(x,t)}{\partial x} + z\dfrac{\partial \Phi(x,t)}{\partial x}\right) = \left(\dfrac{\nu}{1-\nu}\right)\sigma_{xx} & (TBT) \end{cases} \quad (10b)$$

$$\sigma_{xz} = \begin{cases} 2\mu\varepsilon_{xz} = 0 & (EBBT) \\ 2\kappa\mu\varepsilon_{xz} = \dfrac{\kappa E}{2(1+\nu)}\left(\dfrac{\partial \mathrm{w}(x,t)}{\partial x} + \Phi(x,t)\right) & (TBT) \end{cases} \quad (10c)$$

with $\hat{E} = 2\mu + \lambda$ is the equivalent modulus of elasticity, k is the shear correction factor, σ_{xx} and σ_{xz} denote to the components of the Cauchy normal and shear stress components, respectively, λ and μ are Lame's constants in classical elasticity which are related to the elasticity modulus and Poisson's ratio as

$$\mu = \frac{E}{2(1+\nu)}, \qquad \lambda = \frac{\nu E}{(1+\nu)(1-2\nu)} \quad (11)$$

3.3 The surface elasticity theory

According to the surface elasticity theory, developed by Gurtin and Murdoch (1975,1978), the surface layer of an elastic material satisfies distinct constitutive equations involving surface elastic constants and surface residual stress. The non-zero components of the surface stresses are, Mahmoud et al. (2012)

$$\tau_{xx} = \begin{cases} \tau_s + (2\mu_s + \lambda_s)\left(\dfrac{\partial u_o(x,t)}{\partial x} - z\dfrac{\partial^2 \mathrm{w}(x,t)}{\partial x^2}\right) & (EBBT) \\ \tau_s + (2\mu_s + \lambda_s)\left(\dfrac{\partial u_o(x,t)}{\partial x} + z\dfrac{\partial \Phi(x,t)}{\partial x}\right) & (TBT) \end{cases} \quad (12a)$$

$$\tau_{zx} = \tau_s n_z \frac{\partial \mathrm{w}(x,t)}{\partial x} \quad (12b)$$

where n_z is the z-component of the unit outward normal vector to the beam lateral surface. μ_s and λ_s are the surface elastic constants and τ_s is the residual surface stress (i.e., the surface stress at zero strain). τ_{zx} is the out-of-plane components of the surface stress tensor. In order to satisfy the surface conditions of the Gurtin Murdoch model, it is assumed that σ_{zz} varies linearly through the thickness of nanobeam and satisfies the balance conditions on the surfaces, Lu *et al.* (2018). Therefore, σ_{zz} is given for both EBBT and TBT as follows, Eltaher *et al*. (2013b)

$$\sigma_{zz} = \frac{1}{2}(\sigma_{xz}^{s+} - \sigma_{xz}^{s-}) + \frac{z}{h}(\sigma_{xz}^{s+} + \sigma_{xz}^{s-}) \tag{13}$$

σ_{xz}^{s+} and σ_{xz}^{s-} are the top and bottom fibers' stresses, respectively. By substituting Eqs. (10) into Eq. (13), σ_{zz} can be obtained as;

$$\begin{aligned}\sigma_{zz} &= \frac{1}{2}\left(\tau_{nx,x}^{+} + \tau_{nx,x}^{-}\right) + \frac{z}{h}\left(\tau_{nx,x}^{+} - \tau_{nx,x}^{-}\right)\\ &= \frac{1}{2}\left(\tau_s w_{z,xx}^{+} - \tau_s w_{z,xx}^{-}\right) + \frac{z}{h}\left(\tau_s w_{z,xx}^{+} + \tau_s w_{z,xx}^{-}\right)\end{aligned} \tag{14}$$

Eq. (14) can be simplified as

$$\sigma_{zz} = \frac{2z}{h}\left(\tau_s \frac{\partial^2 w(x,t)}{\partial x^2}\right) \tag{15}$$

By using the expression for σ_{zz}, the components of stress for the bulk of nanobeam can be modified as

$$\sigma_{xx} = \hat{E}\varepsilon_{xx} + \nu\sigma_{zz} =$$

$$\begin{cases} \hat{E}\left(\frac{\partial u_o(x,t)}{\partial x} - z\frac{\partial^2 w(x,t)}{\partial x^2}\right) + \frac{2\nu z}{h}\left(\tau_s \frac{\partial^2 w(x,t)}{\partial x^2}\right) & EBBT \\ \hat{E}\left(\frac{\partial u_o(x,t)}{\partial x} + z\frac{\partial \Phi(x,t)}{\partial x}\right) + \frac{2\nu z}{h}\left(\tau_s \frac{\partial^2 w(x,t)}{\partial x^2}\right) & TBT \end{cases} \tag{16}$$

3.4 Equilibrium equations of perforated beams

According to EBBT the equilibrium equations of perforated nanobeams with surface energy effects can be written as

$$\left[\left(\hat{E}I\right)_{eq} - \frac{2\nu h}{12}(A\tau_s)_{eq} + \left(E_s I_p\right)_{eq}\right]\frac{d^4 w}{dx^4} - \left[\frac{2(A\tau_s)_{eq}}{h} - P_o\right]\frac{d^2 w}{dx^2} + q \;\; = 0 \tag{17}$$

Considering the TBT, the equilibrium equations can be expressed as

$$\frac{2\nu}{h}(I\tau_s)_{eq}\frac{d^3 w}{dx^3} + \left[\left(\hat{E}I\right)_{eq} + \left(E_s I_p\right)_{eq}\right]\frac{d^2\Phi}{dx^2} - \kappa(GA)_{eq}\left(\Phi + \frac{dw}{dx}\right) = 0 \tag{18a}$$

$$\left(\frac{2}{h}(A\tau_s)_{eq} + \kappa(GA)_{eq} - P_0\right)\frac{d^2 w}{dx^2} + \kappa(GA)_{eq}\frac{d\Phi}{dx} + q = 0 \tag{18b}$$

Assuming rectangular cross-sectional area of the perforated nanobeam

$$\left(E_s I_p\right)_{eq} = E_s\left(\frac{(A)_{eq}h}{2} + \frac{h^3}{6}\right) \qquad \& \qquad (I\tau_s)_{eq} = \frac{h^2}{12}\;\;(A\tau_s)_{eq} \tag{19}$$

4. Analytical solution

In this section, closed form solutions for static deflection profile throughout the perforated nanobeam with different nonclassical boundary conditions considering both PEBBT and PTBT theories are presented.

4.1 Critical buckling load for PEBNBs

To develop a closed form solution for both the critical buckling load of PEBNBs, the components of both displacement and rotation can expressed in the following generalized form that satisfies all boundary conditions:

$$w(x) = \sum_{n=1}^{\infty} W_n \sin(\alpha x) \qquad \varphi(x) = \textstyle\sum_{n=1}^{\infty}\Phi_n \cos(\alpha x) \tag{20b}$$

Where

$$\alpha = \begin{cases} \left(\frac{n\pi}{L}\right) & (S-S) \\ \left(\frac{(2n+1)\pi}{2L}\right) & (C-C) \\ \left(\frac{(2n-1)\pi}{2L}\right) & (C-F) \end{cases} \tag{20b}$$

Substituting with Eqs. (20) in the governing equations of different beam theories, the critical buckling load of nanobeams considering the surface energy effects can be obtained by solving the resulting eigenvalue problems as

$$\left[-\left(\hat{E}I\right)_{eq} + \frac{2\nu h}{12}(A\tau_s)_{eq} - E_s\left(\frac{(A)_{eq}h}{2} + \frac{h^3}{6}\right)\right]\frac{d^4 w}{dx^4} + \left[\frac{2(A)_{eq}}{h}\tau_s - P_{cr}\right]\frac{d^2 w}{dx^2} = 0 \tag{21a}$$

$$\sum_{n=1}^{\infty}((\alpha)^2 D_E - K_{sE} + N_{0PEBNB})(\alpha)^2 W_n \sin(\alpha x) = 0 \tag{21b}$$

$$D_E = \left[-\left(\hat{E}I\right)_{eq} + \frac{2\nu h}{12}(A\tau_s)_{eq} - E_s\left(\frac{(A)_{eq}h}{2} + \frac{h^3}{6}\right)\right], \text{and} \qquad K_{sE} = \left(\frac{2(A)_{eq}}{h}\right)\tau_s \tag{21c}$$

$$(P_{cr})_{PEBNB} = K_{sE} - (\alpha)^2 D_E \tag{21d}$$

4.2 Critical buckling load for PTNBs

The critical buckling load of the PTNBs can be obtained by substituting Eq. (20) into Eqs. (18), thus one can write

$$0 = -\sum_{n=1}^{\infty}[(\alpha)^3 K_{ST1} + (\alpha)K_{shT}]W_n \cos(\alpha x) - \sum_{n=1}^{\infty}[(\alpha)^2 D_T + K_{shT}]\;\;\Phi_n \cos(\alpha x) \tag{22a}$$

$$0 = -\sum_{n=1}^{\infty}(\alpha)^2(K_{ST2} + K_{shT} - P_{cr})W_n \sin(\alpha x) - \sum_{n=1}^{\infty}(\alpha)K_{shT}\;\Phi_n \sin(\alpha x) \tag{22b}$$

$$K_{ST1} = \frac{2\nu h(A)_{eq}\tau_s}{12}, \qquad K_{ST2} = \frac{2(A)_{eq}}{h}\tau_s, \tag{22c}$$

$$D_T = \left[(\hat{E}I)_{eq} + \left(\frac{(A)_{eq}h}{2} + \frac{h^3}{6}\right)E_s\right],$$

$$K_{shT} = \kappa(GA)_{eq}$$

Eqs. (22(a)) and (22(b)) can be written as

$$\begin{bmatrix} [(\alpha)^3 K_{ST1} + (\alpha)K_{shT}] & [(\alpha)^2 D_T + K_{shT}] \\ [(\alpha)^2 (K_{ST2} + K_{shT} - P_{cr})] & (\alpha)K_{shT} \end{bmatrix} \begin{Bmatrix} W_n \\ \Phi_n \end{Bmatrix} = \begin{Bmatrix} 0 \\ 0 \end{Bmatrix} \quad (23)$$

The critical buckling load can be obtained from the following characteristic equation

$$\frac{[(\alpha)^3 K_{ST1} + (\alpha)K_{shT}][(\alpha)K_{shT}]}{(\alpha)^2[(\alpha)^2 D_T + K_{shT}]} - (K_{ST2} + K_{shT} - P_{cr}) = 0 \quad (24a)$$

$$(P_{cr})_{PTNBs} = K_{ST2} + K_{shT} - \frac{[(\alpha)^2 K_{ST1} + K_{shT}][K_{shT}]}{[(\alpha)^2 D_T + K_{shT}]} \quad (24b)$$

5. Numerical results

5.1 Model Validation

Within this section, the validity of the developed analytical procedure is verified by comparing the obtained results for both the critical buckling load of simply supported nanobeams with the corresponding results obtained by Ansari and Sahmani (2011). Consider a simply supported solid nanobeam having a slenderness ratio; (L/h) ranged from 10 to 50, width of $w=h=$ 1 nm. The beam is made of iron with the following bulk characteristics are E=177.3 GPa, ν=0.27, and ρ=7000 kg/m^3. The surface characteristics are; τ^s=1.7 N/m, u_s=2.5 N/m, λ_s=-8 N/m.

Table 1 Classical and non-classical critical buckling loads corresponding to the lowest three buckling modes for simply supported nanobeams EBBT (nN)

(L/h)	**Ansari and Sahmani (2011)**		**Present**	
	EBBT			
	CL	NCL	CL	NCL
Critical buckling load for the 1st mode (nN)				
10	1.4582	4.6039	1.4582	4.6533
20	0.3646	3.7010	0.3646	3.7133
30	0.1620	3.5338	0.1620	3.5393
40	0.0911	3.4752	0.09114	3.4783
50	0.0583	3.4482	0.05833	3.4501
Critical buckling load for the 2nd mode (nN)				
10	5.8329	8.2158	5.8329	8.4132
20	1.4582	4.6039	1.4582	4.6533
30	0.6481	3.9351	0.6481	3.9570
40	0.3646	3.7010	0.3646	3.7133
50	0.2333	3.5926	0.2333	3.6005
Critical buckling load for the 3rd mode (nN)				
10	13.1241	14.2355	13.1241	14.6796
20	3.2810	6.1089	3.2810	6.2199
30	1.4582	4.6039	1.4582	4.6533
40	0.8203	4.0772	0.8203	4.1050
50	0.5250	3.8334	0.5250	3.8512

Table 2 Classical and non-classical critical buckling loads corresponding to the lowest three buckling modes for simply supported nanobeams TBT (nN)

(L/h)	**Ansari and Sahmani (2011)**		**Present**	
	TBT			
	CL	NCL	CL	NCL
Critical buckling load for the 1st mode (nN)				
10	1.4226	4.5549	1.4226	4.6267
20	0.3623	3.6932	0.3623	3.7116
30	0.1616	3.5307	0.1616	3.5389
40	0.0910	3.4736	0.0910	3.4782
50	0.0583	3.4471	0.0583	3.4501
Critical buckling load for the 2nd mode (nN)				
10	5.3013	7.7531	5.3013	8.0132
20	1.4226	4.5549	1.4226	4.6267
30	0.6410	3.9192	0.6410	3.9517
40	0.3623	3.6932	0.3623	3.7116
50	0.2324	3.5880	0.2324	3.5998
Critical buckling load for the 3rd mode (nN)				
10	10.7081	12.3356	10.7081	12.8384
20	3.1058	5.9339	3.1058	6.0888
30	1.4226	4.5549	1.4226	4.6267
40	0.8089	4.0555	0.8089	4.0965
50	0.5203	3.8213	0.5203	3.8477

The developed procedure is applied to obtain both the critical buckling load for simply supported nanobeam for filling ratio, α=1 (fully filled) for classical (CL) and non-classical (NCL) cases using the following beams theories: EBBT and TBT. The obtained critical buckling loads for the lowest three bucking modes and that obtained by Ansari and Sahmani (2011) are shown in Tables 1 and 2. It is noticed that good agreement is found between the obtained results and that obtained by Ansari and Sahmani (2011) for the three buckling modes for the two considered beams theories.

5.2 Buckling analysis

Variations of the lowest buckling load with the perforated beam filling ratio at N =4 for different boundary conditions (BCs) for both classical and nonclassical analysis are illustrated in Fig. 1. It may be seen that, for both classical and nonclassical analysis, the magnitude of the critical buckling loads are increased with increasing the filling ratio for both PEBBT and PTBT due to increasing the beam rigidity. Also, the deviation between the nonclassical and classical values of the critical buckling loads is increased with increasing beam filling ratio. Moreover, the magnitude of these loads are significantly influenced by the presence of surface effects. Depending on the material surface characteristics, the critical buckling loads could either be increased or decreased compared to the corresponding classical values. Additionally, it could be seen that the boundary conditions significantly affect the critical buckling load, smaller values of the nonclassical buckling load (P_{cr}[NCL])are obtained compared to the corresponding classical values (P_{cr}[CL]) for clamped – clamped (C_C) BCs while higher values of (P_{cr}[NCL]) are detected for both clamped -free(C_F) and Simply supported (S_S) BCs compared with the corresponding classical values (P_{cr}[CL]).

Additionally, higher deviation between the nonclassical and classical values of P_{cr} is detected for C_F compared to that obtained for both C_C and S_S boundary conditions (BCs). Moreover, the surface residual stress, τ^s has a significant effect on the critical buckling load compared with that of the surface elasticity modulus, E_s. It is also noticed that, for the considered slenderness ratio (L/h=10), smaller values of the critical buckling loads are obtained for PTBT compared to the PEBBT due to the shear deformation effect. The slenderness ratio significantly affects the critical buckling loads. The dependency of the lowest critical buckling loads on the perforated beam filling ratio for both PEBBT and PTBT at (L/h=40) at different boundary conditions is illustrated in Fig. 2. Increasing the beam perforated beam slenderness ratio (L/h=40) results in smaller values of the corresponding critical buckling loads of thick perforated beams (L/h=10). On the other hand, the shift between the classical and nonclassical critical buckling loads is increased due to increasing perforated beam surface area. Moreover, for thin beams (L/h=40) both PEBBT and PTBT give almost the same values of the critical buckling loads for C_F and S_S boundary conditions while small deviation is detected for C_C boundary conditions.

Dependency of the critical buckling loads on the number of hole rows (N) at a fixed value of filling ratio (α=0.5) is illustrated in Fig. 3. It is seen that for both beams' theories, the magnitude of the critical buckling loads is decreased with increasing the number of hole rows for both classical and nonclassical analysis due to the decrease of the beam rigidity. Moreover, due to the shear deformation effect, smaller values of the critical buckling loads are obtained for PTBT compared to the corresponding PEBBT. On the other hand, the surface elasticity and the surface residual stress are significantly affect the critical buckling loads for both PEBBT and PTBT. Large deviation between the nonclassical and classical critical buckling loads is detected because of residual stress compared with that obtained due to the surface elasticity. Also, the boundary conditions significantly affect the magnitude and deviation between the nonclassical and classical critical buckling loads. Higher deviation is detected for C_F compared to both C_C and S_S boundary conditions.

To demonstrate the effect of slenderness ratio on the critical buckling load, the critical buckling load is detected for perforated beams with slenderness ratio of (L/h=40), as illustrated in Fig. 4. It may be noticed that both PEBBT and PTBT results in the same critical bulking loads for S_S and C_F BCs while small deviation is still found for C_C BCs. Moreover, the deviation between the classical and nonclassical critical buckling loads is increased by increasing the perforated beam slenderness ratio due to increasing the perforated beam surface area to bulk volume ratio.

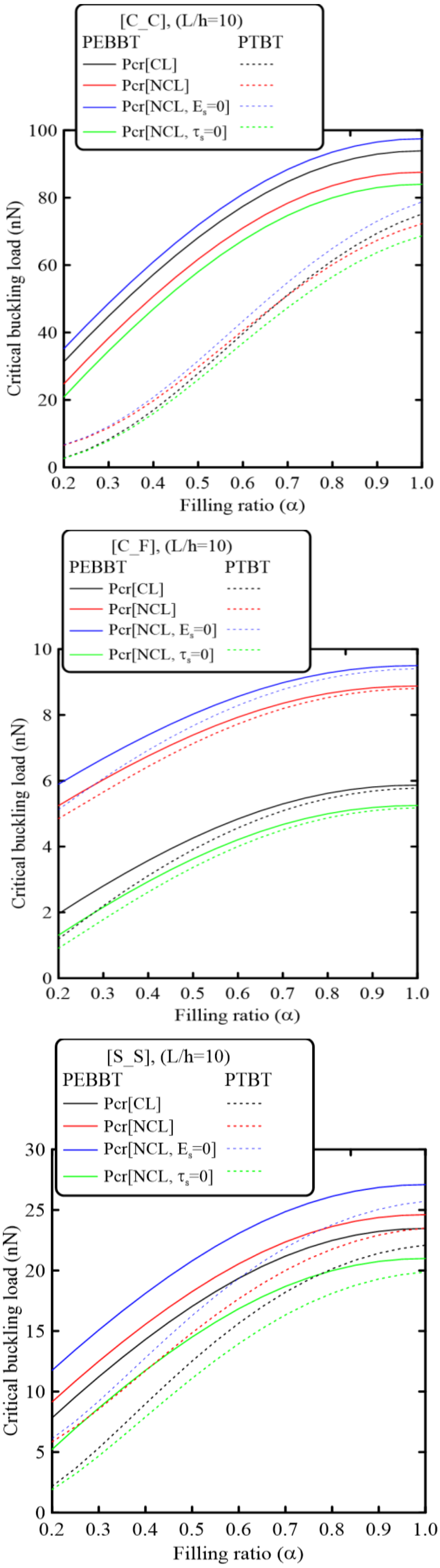

Fig. 1 Variation of the critical buckling load with the filling ratio for both PEBBT and PTBT for different BCs at L/H=10

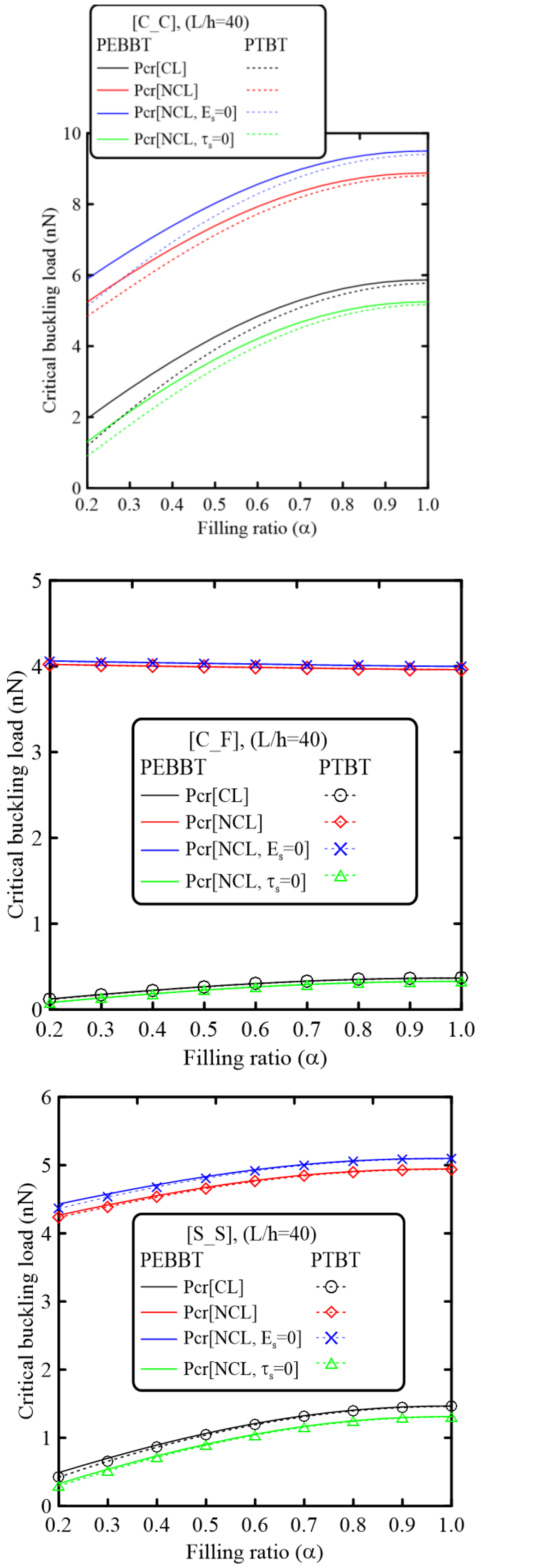

Fig. 2 Variation of the critical buckling load with the filling ratio for both PEBBT and PTBT for different BCs at L/H=40

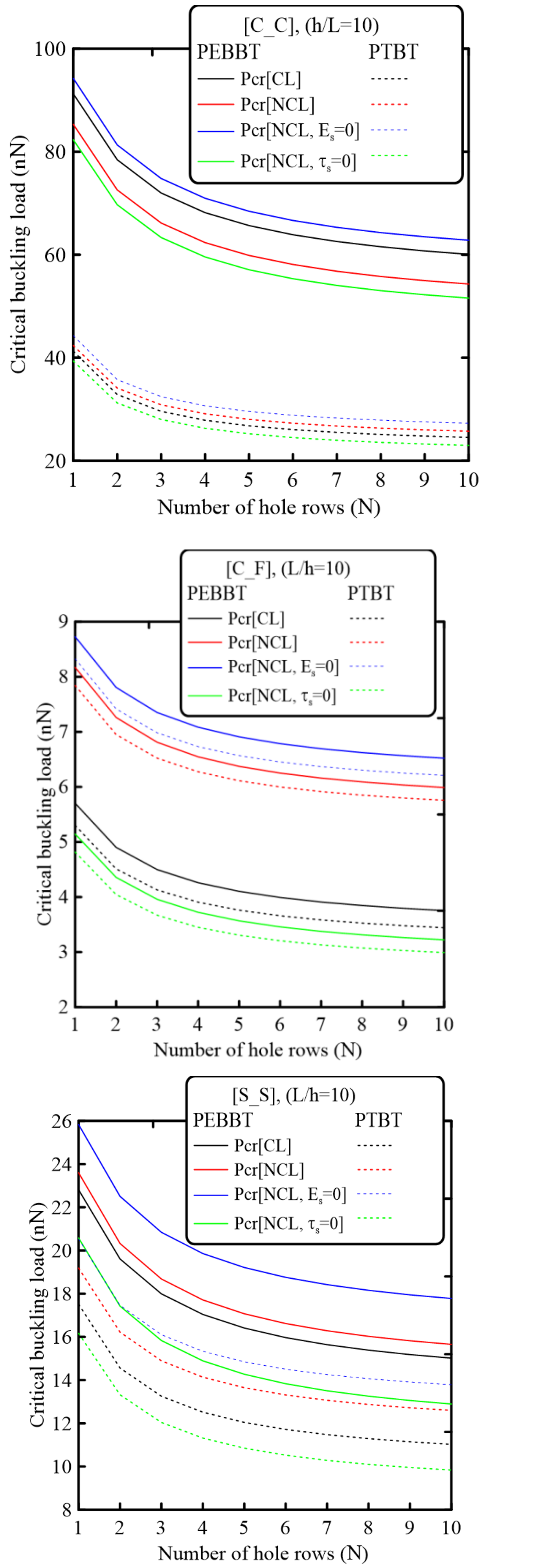

Fig. 3 Variation of the critical buckling load with the number of hole rows for both PEBBT and PTBT for different BCs at L/H=10

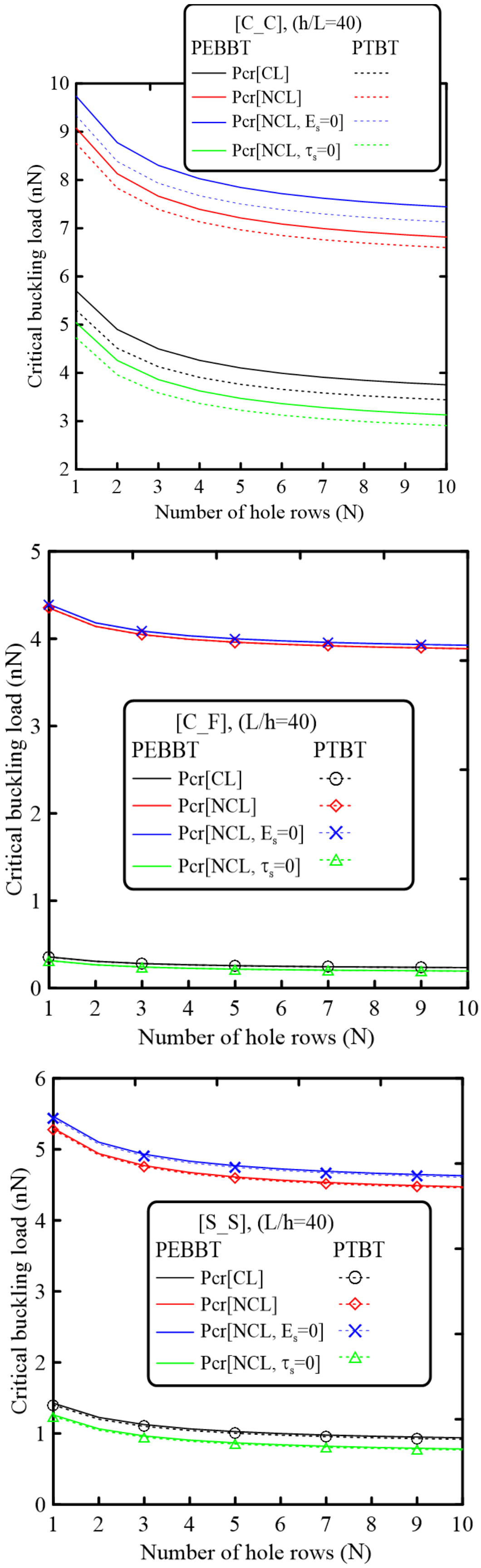

Fig. 4 Variation of the critical buckling load with the number of hole rows for both PEBBT and PTBT for different BCs at L/H=40

6. Conclusions

An analytical methodology capable of investigating the critical buckling for perforated beams incorporating the surface stress effects is presented. The Gurtin-Murdoch (GM) surface elasticity theory is adopted to incorporate the surface energy effects. Regular square holes are considered through perforation process. Both PEBBT and PTBT are considered to explore the shear deformation effect associated with the perforation process. Explicit forms for the non-classical critical buckling loads are developed relevant to each type of beam theory considering different nonclassical boundary and loading conditions. The proposed non-classical procedure is verified by comparing the obtained results with the previous published results and an excellent agreement is obtained. The obtained numerical results revealed the following concluding remarks:

- Surface stresses significantly affect the critical buckling loads. this effect is mainly due to size dependent. The difference of the obtained results obtained based on the nonclassical surface elasticity model and the corresponding results based on classical models relies on the magnitudes of the surface properties.
- Increasing the perforated nanobeam aspect ratio results in increasing the difference between the classical and nonclassical values of critical buckling.
- The surface residual stress, τ has more significant effect on the critical buckling loads with the corresponding effect of the surface elasticity, Es.
- As the number of holes throughout the cross section of the perforated nanobeams increases the lowest critical buckling load decreases due to decreasing the beam bending stiffness.
- The perforated nanobeams filling ratio significantly affects buckling behavior of perforated nanobeams. As the filling ratio increases the lowest critical buckling load increases due to increasing the beam bending stiffness.
- For perforated nanobeams with lower aspect ratio (L/h) the Euler Bernoulli beam theory can't effectively investigate the buckling behavior of perforated nanobeams especially at lower values of filling ratio (α<0.5).
- The nonclassical boundary conditions significantly affect the buckling behaviors of perforated nanobeams.

Acknowledgments

This work was funded by the Deanship of Scientific Research (DSR), King Abdulaziz University, Jeddah, under grant No. (D-058-135-1441). The authors, therefore, acknowledge with thanks DSR technical and financial support.

References

Abdelrahman, A.A., Eltaher, M.A., Kabeel, A.M., Abdraboh, A. M. and Hendi, A.A. (2019), "Free and forced analysis of perforated beams", *Steel Compos. Struct.*, **31**(5), 489-502. DOI: https://doi.org/10.12989/scs.2019.31.5.489.

Ahouel, M., Houari, M.S.A., Bedia, E.A. and Tounsi, A. (2016), "Size-dependent mechanical behavior of functionally graded trigonometric shear deformable nanobeams including neutral surface position concept", *Steel Compos. Struct.*, **20**(5), 963-981. https://doi.org/10.12989/scs.2016.20.5.963.

Almitani, K.H., Abdelrahman, A.A. and Eltaher, M.A. (2019), "On forced and free vibrations of cutout squared beams", *Steel Compos. Struct.*, **32**(5), 643-655. https://doi.org/10.12989/scs.2019.32.5.643.

Almitani, K.H. (2018), "Buckling behaviors of symmetric and antisymmetric functionally graded beams", *J. Appl. Comput. Mech.*, **4**(2), 115-124. 10.22055/JACM.2017.23040.1147.

Ansari, R, and Sahmani, S. (2011), "Bending behavior and buckling of nanobeams including surface stress effects corresponding to different beam theories", *Int. J. Eng. Sci.*, **49**(11), 1244-1255. https://doi.org/10.1016/j.ijengsci.2011.01.007

Barati, M.R. and Zenkour, A.M. (2019), "Thermal post-buckling analysis of closed circuit flexoelectric nanobeams with surface effects and geometrical imperfection", *Mech. Adv. Mater. Struct.*, **26**(17), 1482-1490.https://doi.org/10.1080/15376494.2018.1432821

Bellifa, H., Benrahou, K. H., Bousahla, A. A., Tounsi, A., & Mahmoud, S.R. (2017), "A nonlocal zeroth-order shear deformation theory for nonlinear postbuckling of nanobeams", *Struct. Eng. Mech.*, **62**(6), 695-702. https://doi.org/10.12989/sem.2017.62.6.695

Benahmed, A., Fahsi, B., Benzair, A., Zidour, M., Bourada, F. and Tounsi, A. (2019), "Critical buckling of functionally graded nanoscale beam with porosities using nonlocal higher-order shear deformation", *Struct. Eng. Mech.*, **69**(4), 457-466. https://doi.org/10.12989/sem.2019.69.4.457

Bendali, A., Labedan, R., Domingue, F. and Nerguizian, V. (2006), "Holes effects on RF MEMS parallel membranes capacitors", *Proceedings of the 2006 Canadian Conference on Electrical and Computer Engineering* (pp. 2140-2143). IEEE. DOI: 10.1109/CCECE.2006.277600

Bourouina, H., Yahiaoui, R., Sahar, A. and Benamar, M.E.A. (2016), "Analytical modeling for the determination of nonlocal resonance frequencies of perforated nanobeams subjected to temperature-induced loads", *Physica E*, **75**, 163-168. https://doi.org/10.1016/j.physe.2015.09.014

Bourouina, H., Yahiaoui, R., Kerid, R., Ghoumid, K., Lajoie, I., Picaud, F. and Herlem, G. (2020), "The influence of hole networks on the adsorption-induced frequency shift of a perforated nanobeam using non-local elasticity theory", *J. Phys. Chem. Solids*, **136**, 109201. https://doi.org/10.1016/j.jpcs.2019.109201.

Chaht, F.L., Kaci, A., Houari, M.S.A., Tounsi, A., Bég, O.A. and Mahmoud, S. R. (2015), "Bending and buckling analyses of functionally graded material (FGM) size-dependent nanoscale beams including the thickness stretching effect", *Steel Compos. Struct.*, **18**(2), 425-442. https://doi.org/10.12989/scs.2015.18.2.425.

De Pasquale, G., Veijola, T. and Somà, A. (2009), "Modelling and validation of air damping in perforated gold and silicon MEMS plates", *Journal of Micromechanics and Microengineering*, **20**(1), 015010. ttps://doi.org/10.1088/0960-1317/20/1/015010

Ebrahimi, F., Daman, M. and Fardshad, R.E. (2017), "Surface effects on vibration and buckling behavior of embedded nanoarches", *Struct Eng Mech*, **64**(1), 1-10. https://doi.org/10.12989/sem.2017.64.1.001.

Eltaher, M.A., Emam, S.A. and Mahmoud, F.F. (2013a), "Static and stability analysis of nonlocal functionally graded nanobeams", *Compos. Struct.*, **96**, 82-88. https://doi.org/10.1016/j.compstruct.2012.09.030.

Eltaher, M.A., Mahmoud, F.F., Assie, A.E. and Meletis, E.I. (2013b), "Coupling effects of nonlocal and surface energy on vibration analysis of nanobeams", *Appl. Math. Comput.*, **224**, 760-774. https://doi.org/10.1016/j.amc.2013.09.002.

Eltaher, M.A., Khairy, A., Sadoun, A.M. and, F.A. (2014a), "Static and buckling analysis of functionally graded Timoshenko nanobeams", *Appl. Math. Comput.*, **229**, 283-295. https://doi.org/10.1016/j.amc.2013.12.072.

Eltaher, M.A., Hamed, M.A., Sadoun, A.M. and Mansour, A. (2014b), "Mechanical analysis of higher order gradient nanobeams", *Appl. Math. Comput.*, **229**, 260-272. https://doi.org/10.1016/j.amc.2013.12.076

Eltaher, M.A., Khater, M.E. and Emam, S.A. (2016a), "A review on nonlocal elastic models for bending, buckling, vibrations, and wave propagation of nanoscale beams", *Appl. Math. Model.*, **40**(5-6), 4109-4128. https://doi.org/10.1016/j.apm.2015.11.026.

Eltaher, M.A., Khater, M.E., Park, S., Abdel-Rahman, E. and Yavuz, M. (2016b), "On the static stability of nonlocal nanobeams using higher-order beam theories", *Adv. Nano Res.*, **4**(1), 51. https://doi.org/10.12989/anr.2016.4.1.051.

Eltaher, M.A., Kabeel, A.M., Almitani, K.H. and Abdraboh, A.M. (2018a), "Static bending and buckling of perforated nonlocal size-dependent nanobeams", *Microsyst/ Technologies*, **24**(12), 4881-4893. https://doi.org/10.1007/s00542-018-3905-3.

Eltaher, M.A., Abdraboh, A.M. and Almitani, K.H. (2018b), "Resonance frequencies of size dependent perforated nonlocal nanobeam", *Microsys. Technologies*, **24**(9), 3925-3937. https://doi.org/10.1007/s00542-018-3910-6.

Eltaher, M.A., Mohamed, N., Mohamed, S. and Seddek, L.F. (2019), "Postbuckling of curved carbon nanotubes using energy equivalent model", *J. Nano Res.*, **57**, 136-157. https://doi.org/10.4028/www.scientific.net/JNanoR.57.136.

Eltaher, M.A. and Mohamed N.A., (2020), "Vibration of Nonlocal Perforated Nanobeams under General Boundary Conditions", *Smart Struct. Syst.*, **25**(4). 501-514. https://doi.org/10.12989/sss.2020.25.4.501.

Eltaher, M.A., Mohamed, S.A. and Melaibari, A. (2020a), "Static stability of a unified composite beams under varying axial loads", *Thin-Wall. Struct.*, 147, 106488. https://doi.org/10.1016/j.tws.2019.106488.

Eltaher, M.A., Omar, F.A., Abdraboh, A.M., Abdalla, W.S. and Alshorbagy, A.E. (2020b), "Mechanical Behaviors of Piezoelectric Nonlocal Nanobeam with Cutouts", *Smart Struct. Syst.*, **25**(2), 219-228. https://doi.org/10.12989/sss.2020.25.2.219.

Emam, S.A., Eltaher, M.A., Khater, M.E. and Abdalla, W.S. (2018), "Postbuckling and free vibration of multilayer imperfect nanobeams under a pre-stress load", *Appl. Sci.*, **8**(11), 2238. https://doi.org/10.3390/app8112238.

Foroutan, S., Haghshenas, A., Hashemian, M., Eftekhari, S.A. and Toghraie, D, (2018), "Spatial buckling analysis of current-carrying nanowires in the presence of a longitudinal magnetic field accounting for both surface and nonlocal effects", *Physica E*, **97**, 191-205. https://doi.org/10.1016/j.physe.2017.11.015.

Esmaeili, M. and Beni, T.Y. (2019), "Vibration and buckling analysis of functionally graded flexoelectric smart beam", *J. Appl. Comput. Mech.*, **5**(5), 900-917. 10.22055/JACM.2019.27857.1439.

Fu, Y., Zhang, J. and Jiang, Y. (2010), "Influences of the surface energies on the nonlinear static and dynamic behaviors of nanobeams", *Physica E: Low-dimensional Syst. Nanostruct.*, **42**(9), 2268-2273. https://doi.org/10.1016/j.physe.2010.05.001.

Guha, K., Kumar, M., Agarwal, S. and Baishya, S. (2015), "A modified capacitance model of RF MEMS shunt switch incorporating fringing field effects of perforated beam", *Solid-State Electronics*, **114**, 35-42. https://doi.org/10.1016/j.sse.2015.07.008.

Guha, K., Laskar, N.M., Gogoi, H.J., Borah, A.K., Baishnab, K.L. and Baishya, S. (2017), "Novel analytical model for optimizing the pull-in voltage in a flexured MEMS switch incorporating beam perforation effect", *Solid-State Electronics*, **137**, 85-94. https://doi.org/10.1016/j.sse.2017.08.007.

Gurtin, M.E. and Murdoch, A. I. (1975), "A continuum theory of elastic material surfaces", *Archive for Rational Mechanics and Analysis*, **57**(4), 291-323.

Gurtin, M.E. and Murdoch, A.I. (1978), "Surface stress in solids", *Int. J. Solids Struct.*, **14**(6), 431-440.

Hadipeykani, M., Aghadavoudi, F. and Toghraie, D. (2020), "A molecular dynamics simulation of the glass transition temperature and volumetric thermal expansion coefficient of thermoset polymer based epoxy nanocomposite reinforced by CNT: A statistical study", *Physica A: Statistical Mechanics and its Applications*, 123995. https://doi.org/10.1016/j.physa.2019.123995

Hashemian, M., Foroutan, S. and Toghraie, D. (2019a), "Comprehensive beam models for buckling and bending behavior of simple nanobeam based on nonlocal strain gradient theory and surface effects", *Mechanics of Materials*, **139**, 103209. https://doi.org/10.1016/j.mechmat.2019.103209.

Hashemian, M., Vaez, A.H. and Toghraie, D. (2019b), "Investigation of viscous fluid flow and dynamic stability of CNTs subjected to axial harmonic load coupled using Bolotin's method", *Int. J. Numer. Method. Heat Fluid Fl.*, https://doi.org/10.1108/HFF-12-2018-0739.

Hamed, M.A., Mohamed, S.A. and Eltaher, M.A. (2020), "Buckling analysis of sandwich beam rested on elastic foundation and subjected to varying axial in-plane loads", *Steel Compos. Struct.*, **34**(1), 75-89. https://doi.org/10.12989/scs.2020.34.1.075.

Hamidi, B.A., Hosseini, S.A., Hassannejad, R. and Khosravi, F. (2020), "Theoretical analysis of thermoelastic damping of silver nanobeam resonators based on Green–Naghdi via nonlocal elasticity with surface energy effects", *The European Physical J. Plus*, **135**(1), 1-20. https://doi.org/10.1140/epjp/s13360-019-00037-8.

Jena, S.K., Chakraverty, S., Malikan, M. and Tornabene, F. (2019), "Stability analysis of single-walled carbon nanotubes embedded in winkler foundation placed in a thermal environment considering the surface effect using a new refined beam theory", *Mechanics Based Design of Structures and Machines*, 1-15. https://doi.org/10.1080/15397734.2019.1698437.

Kerid, R., Bourouina, H., Yahiaoui, R., Bounekhla, M. and Aissat, A. (2019), "Magnetic field effect on nonlocal resonance frequencies of structure-based filter with periodic square holes network", *Physica E: Low-dimensional Systems and Nanostructures*, **105**, 83-89. https://doi.org/10.1016/j.physe.2018.05.021.

Khabaz, M.K., Eftekhari, S.A., Hashemian, M. and Toghraie, D. (2020), "Optimal vibration control of multi-layer micro-beams actuated by piezoelectric layer based on modified couple stress and surface stress elasticity theories", *Physica A: Statistical Mechanics and its Applications*, 123998. https://doi.org/10.1016/j.physa.2019.123998.

Khater, M.E., Eltaher, M.A., Abdel-Rahman, E. and Yavuz, M. (2014), "Surface and thermal load effects on the buckling of curved nanowires", *Eng. Sci. Technol.*, **17**(4), 279-283. https://doi.org/10.1016/j.jestch.2014.07.003.

Lu, L., Guo, X. and Zhao, J. (2018), "On the mechanics of Kirchhoff and Mindlin plates incorporating surface energy", *Int. J. Eng. Sci.*, **124**, 24-40. https://doi.org/10.1016/j.ijengsci.2017.11.020.

Luschi, L. and Pieri, F. (2014), "An analytical model for the determination of resonance frequencies of perforated beams", *J. Micromech. Microeng.*, **24**(5), 055004. https://doi.org/10.1088/0960-1317/24/5/055004.

Luschi, L. and Pieri, F. (2016), "An analytical model for the resonance frequency of square perforated Lamé-mode resonators", *Sensors Actuat. B: Chemical*, **222**, 1233-1239. https://doi.org/10.1016/j.snb.2015.07.085.

Mahmoud, F.F., Eltaher, M.A., Alshorbagy, A.E. and Meletis, E.I. (2012), "Static analysis of nanobeams including surface effects by nonlocal finite element", *J. Mech. Sci. Technol.*, **26**(11), 3555-3563. https://doi.org/10.1007/s12206-012-0871-z

Malikan, M. and Eremeyev, V.A. (2020), "Post-critical buckling of truncated conical carbon nanotubes considering surface effects embedding in a nonlinear Winkler substrate using the Rayleigh-Ritz method", *Materials Research Express*.

Mercan, K. and Civalek, Ö. (2017), "Buckling analysis of Silicon carbide nanotubes (SiCNTs) with surface effect and nonlocal elasticity using the method of HDQ", *Compos. Part B: Eng.*, **114**, 34-45. https://doi.org/10.1016/j.compositesb.2017.01.067.

Mirkalantari, S.A., Hashemian, M., Eftekhari, S.A. and Toghraie, D. (2017), "Pull-in instability analysis of rectangular nanoplate based on strain gradient theory considering surface stress effects", *Physica B: Condensed Matter*, **519**, 1-14. https://doi.org/10.1016/j.physb.2017.05.028

Mohamed, N., Eltaher, M.A., Mohamed, S.A. and Seddek, L.F. (2019), "Energy equivalent model in analysis of postbuckling of imperfect carbon nanotubes resting on nonlinear elastic foundation", *Struct. Eng. Mech.*, **70**(6), 737-750. https://doi.org/10.12989/sem.2019.70.6.737.

Mohamed, N., Mohamed, S.A. and Eltaher, M.A. (2020), "Buckling and post-buckling behaviors of higher order carbon nanotubes using energy equivalent mode", *Engineering with Computer*,1-14. https://doi.org/10.1007/s00366-020-00976-2.

Mohammadimehr, M., Mehrabi, M., Hadizadeh, H. and Hadizadeh, H. (2018), "Surface and size dependent effects on static, buckling, and vibration of micro composite beam under thermo-magnetic fields based on strain gradient theory", *Steel Compos. Struct.*, **26**(4), 513-531. https://doi.org/10.12989/scs.2018.26.4.513.

Ouakad, H.M., Sedighi, H.M. and Younis, M.I. (2017), "One-to-one and three-to-one internal resonances in MEMS shallow arches", *J. Comput. Nonlinear Dynam.*, **12**(5), 051025. https://doi.org/10.1115/1.4036815.

Oveissi, S., Nahvi, H., and Toghraie, D. (2015), "Axial wave propagation analysis in fixed and dynamic of carbon nanotubes conveying fluid", *Solid Mech. Eng.*, **8**(2), 108-115.

Oveissi, S., Eftekhari, S.A., & Toghraie, D. (2016a), "Longitudinal vibration and instabilities of carbon nanotubes conveying fluid considering size effects of nanoflow and nanostructure", *Physica E*, **83**, 164-173. https://doi.org/10.1016/j.physe.2016.05.010

Oveissi, S., Toghraie, D. and Eftekhari, S.A. (2016b), "Longitudinal vibration and stability analysis of carbon nanotubes conveying viscous fluid", *Physica E*, **83**, 275-283. https://doi.org/10.1016/j.physe.2016.05.004.

Oveissi, S., Toghraie, D.S. and Eftekhari, S.A. (2017), "Analysis of transverse vibrational response and instabilities of axially moving CNT conveying fluid", *Int. J. Fluid Mech. Res.*, **44**(2). DOI: 10.1615/InterJFluidMechRes.2017016740.

Oveissi, S., Toghraie, D.S. and Eftekhari, S.A. (2018), "Investigation on the effect of axially moving carbon nanotube, nanoflow, and Knudsen number on the vibrational behavior of the system", *Int. J. Fluid Mech. Res.*, **45**(2). 10.1615/InterJFluidMechRes.2018021036.

Pirmoradian, M., Torkan, E., Abdali, N., Hashemian, M. and Toghraie, D. (2020), “Thermo-mechanical stability of single-layered graphene sheets embedded in an elastic medium under action of a moving nanoparticle”, *Mech. Mater.*, **141**, 103248. https://doi.org/10.1016/j.mechmat.2019.103248.

Pirmoradian, M., Torkan, E. and Toghraie, D. (2020b), “Study on size-dependent vibration and stability of DWCNTs subjected to moving nanoparticles and embedded on two-parameter foundations”, *Mech. Mater.*, **142**, 103279. https://doi.org/10.1016/j.mechmat.2019.103279.

Rao, K.S., Sailaja, B.V.S., Sravani, K.G., Vineetha, K.V., Kumar, P.A., Prathyusha, D. and Guha, K. (2019), “New Analytical Capacitance Modeling of the Perforated Switch Considering the Fringing Effect”, *IEEE Access*, **7**, 27026-27036. 10.1109/ACCESS.2018.2889724.

Rebeiz, G. M. (2004). *RF MEMS: theory, design, and technology*. John Wiley & Sons.

Saffari, S., Hashemian, M. and Toghraie, D. (2017), “Dynamic stability of functionally graded nanobeam based on nonlocal Timoshenko theory considering surface effects”, *Physica B: Condensed Matter*, **520**, 97-105. https://doi.org/10.1016/j.physb.2017.06.029.

Sedighi, H.M. and Daneshmand, F. (2014), “Nonlinear transversely vibrating beams by the homotopy perturbation method with an auxiliary term”, *J. Appl. Comput. Mech.*, **1**(1), 1-9. 10.22055/jacm.2014.10545.

Sedighi, H.M. and Bozorgmehri, A. (2016), “Dynamic instability analysis of doubly clamped cylindrical nanowires in the presence of Casimir attraction and surface effects using modified couple stress theory”, *Acta Mechanica*, **227**(6), 1575-1591. https://doi.org/10.1007/s00707-016-1562-0.

Shen, J.P., Li, C., Fan, X.L. and Jung, C.M. (2017), “Dynamics of silicon nanobeams with axial motion subjected to transverse and longitudinal loads considering nonlocal and surface effects”, *Smart Struct. Syst.*, **19**(1), 105-113. https://doi.org/10.12989/sss.2017.19.1.105.

Yang, F.A.C.M., Chong, A.C.M., Lam, D.C.C. and Tong, P. (2002), “Couple stress-based strain gradient theory for elasticity”, *Int. J. Solids Struct.*, **39**(10), 2731-2743. https://doi.org/10.1016/S0020-7683(02)00152-X.

Yousefzadeh, S., Akbari, A., Najafi, M., Akbari, O.A. and Toghraie, D. (2019), “Analysis of buckling of a multi-layered nanocomposite rectangular plate reinforced by single-walled carbon nanotubes on elastic medium considering nonlocal theory of Eringen and variational approach”, *Indian J. Physics*, 1-15. https://doi.org/10.1007/s12648-019-01546-z.

Wang, L. (2012), “Surface effect on buckling configuration of nanobeams containing internal flowing fluid: A nonlinear analysis”, *Physica E: Low-dimensional Systems and Nanostructures*, **44**(4), 808-812. https://doi.org/10.1016/j.physe.2011.12.006.

CC